Sisyphus: Redefining Low Power for LoRa Receiver

Han Wang
University of Electronic Science
and Technology of China
wang_han@std.uestc.edu.cn

Yihang Song
University of Electronic Science
and Technology of China
songyihang@uestc.edu.cn

Qianhe Meng
University of Electronic Science
and Technology of China
qianhe@std.uestc.edu.cn

Zetao Gao
University of Electronic Science
and Technology of China
zetaogao@std.uestc.edu.cn

Chong Zhang
University of Electronic Science
and Technology of China
Southwest Petroleum University
zhangchong92@swpu.edu.cn

Li Lu[*]
University of Electronic Science
and Technology of China
luli2009@uestc.edu.cn

ABSTRACT

Legacy LoRa receiver adopts a superheterodyne architecture with a runtime power consumption of up to 100mW, resulting in its low-power promise can only be delivered in low duty-cycle mode. This paper presents *Sisyphus* as an ultra-low-power LoRa receiver, ensuring around-the-clock LoRa availability while extending battery life significantly. To achieve this, we propose a novel receiver design for passive coherent demodulation of LoRa. In this design, we creatively couple LoRa's down-conversion with de-chirping (dc^2), leveraging the processing gain brought by chirp spread spectrum (CSS) modulation to boost communication range without the need for additional power supply. Moreover, we exploit the cyclical time-frequency feature intrinsic to LoRa for demodulation, and a low-power analog-digital signal processing circuit with negligible power is devised to replace the existing power-intensive sampling and costly digital computation. We prototype Sisyphus for proof-of-concept, and comprehensive experimental results demonstrate that Sisyphus can achieve significant power savings compared to legacy LoRa receiver while retaining the anti-interference ability of legacy LoRa. We envision that the design of Sisyphus can unlock the potential for broader applications of LoRa.

[*]Li Lu is the corresponding author to this paper.

CCS CONCEPTS

• **Hardware** → **Wireless devices**; • **Networks** → **Wireless access points, base stations and infrastructure**.

KEYWORDS

LoRa receiver, Ultra-low-power communication, IoT

1 INTRODUCTION

LoRa, a representative low-power wide area network (LP-WAN) technology, holds the potential as a key cog in building ubiquitously connected world. The projection [1] indicates that the market for LoRa devices is expected to reach USD 5.7 billion by 2024, experiencing a remarkable compound annual growth rate of 35.6% from 2024 to 2034.

Despite the promising outlook, a pressing challenge arises: *LoRa's claimed low power practically can only be realized in low duty-cycle mode.* Our empirical evaluation reveals that the SX1278-based [2] LoRa module consumes approximately 400mW during transmission at 20dBm and up to 100mW during reception. There are varieties of application scenarios that demand around-the-clock and real-time remote monitoring while utility power is not always available, such as industrial IoT (IIoT) [3], forest fire alarm [4], and sensor-free sensing in the wild [5]. Whereas the battery-powered LoRa device's energy budget is extremely tight. For instance, an AA 1.5V battery typically offers a capacity ranging from 500 to 3000mAh and a coin battery (like CR2032 [6]) has a typical capacity of only 225mAh. That is, when leaving the device running continuously, its equipped power supply can

only sustain operation for a matter of hours to days. The replacements of batteries have to be conducted very frequently, posing a tough challenge to the maintenance cost of LoRa devices.

Therefore, the runtime energy consumption of LoRa must be emphasized. Recent efforts have been directed towards combining LoRa with backscatter communication to reduce the power of uplink transmission [7–12]. These endeavors involve offloading the carrier generation burden to an external carrier emitter, thereby circumventing the power-intensive components of a typical active radio, leading to significant power savings. Thus, the bottleneck in power reduction for LoRa devices has shifted from the uplink to the downlink.

Turning our attention to the downlink, the underlying reason for the power-consuming nature of legacy LoRa downlink stems from its reliance on a *superheterodyne* architecture. This intricate architecture encompasses a complex reception process, including analog down-conversion from radio frequency (RF) to intermediate frequency (IF), sampling, digital down-conversion (DDC) from IF to baseband, de-spreading (*a.k.a.*, de-chirping), fast Fourier transform (FFT) and peak detection. These elaborate operations necessitate the equipment of power-hungry components such as local oscillators (LO), phase-locked loops (PLL), multi-bit analog-to-digital converters (ADC), and on-board digital baseband processors (DBP), collectively contributing to no less than 70% of the total power. Saiyan [13] tries to reduce power of LoRa receiver and proposes to reshape the envelope of LoRa using surface acoustic wave (SAW) filter, and perform demodulation on the reshaped envelope. However, it does not engage with the de-chirping of LoRa, which is the crux of harnessing processing gain brought by CSS modulation and further LoRa's long-range performance. So Saiyan essentially functions as a passive frequency shift keying (FSK) receiver. To keep its communication range, Saiyan has to use amplifiers consuming extensive power [14, 15], which is surprisingly higher than that of legacy LoRa receiver.

In this paper, we ask the following question: *Can we replace the power-hungry components in legacy LoRa receiver with their passive/low-power counterparts while retaining the processing gain brought by CSS modulation?* A positive answer would pave the way to a thorough power reduction of LoRa receiver. Intuitively, we may remove on-device LO and PLL as prior works do [16, 17], which employ a helper device or RF chain to emit an unmodulated (single-tone) carrier (we refer to it as helper signal) at the utility-powered gateway side and perform passive down-conversion at the battery-powered receiver side. This approach only focuses on the power issue of down-conversion, however, IF sampling and computationally expensive baseband operations (*i.e.*, de-chirping, FFT, etc.) are still required on the receiver, which leaves a large amount of room for power reduction.
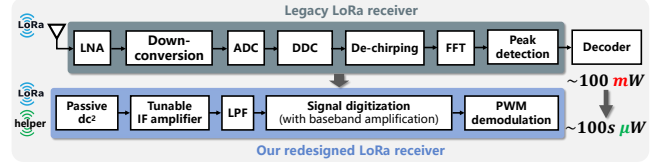
Figure 1: Redesign of LoRa receiver, which allows us to achieve ultra-low-power LoRa reception while retaining the processing gain of CSS modulation.

To settle the untouchable power reduction room, we rethink the legacy LoRa receiver design and present *Sisyphus*, the first passive LoRa receiver to obtain CSS processing gain. As Figure 1 shows, we redesign the reception process of the LoRa signal. Firstly, we revisit the cyclical frequency shifting feature of LoRa chirp, which indicates the possibility of converting the demodulation scheme from initial frequency tracking into cyclical frequency shifting time localization. This evades the need for operation in frequency domain in favor of time domain, allowing us to replace those computationally expensive operations with low-power analog signal processing. Based on our demodulation scheme, we propose an innovative framework to remove those power-hungry components. Specifically, we rely on the abundant computation resources and unconstrained power of the gateway and let the unmodulated helper signal be modulated into a chirp signal for de-chirping of LoRa as well, thus signal down-conversion and de-chirping can be seamlessly integrated and achieved with zero on-device energy consumption, ensuring Sisyphus can obtain CSS modulation's processing gain. Then we devise an analog-digital signal processing method to conduct the proposed demodulation on the post-dc^2 signal with negligible energy consumption. Furthermore, we bypass the power-consuming low noise amplifier (LNA) in legacy receiver and employ low-power alternatives including bipolar junction transistors (BJT) based tunable IF amplifier and baseband low-power operational amplifier (OPA) to improve the link budget. In contrast to legacy receiver, we have not only eliminated LO and PLL but also revolutionized the legacy LoRa reception process, greatly squeezing the energy budget of LoRa receiver. To put Sisyphus into practice, however, we must address the following technical challenges.

First, the legacy de-chirping operation of LoRa is to employ a base down-chirp to be multiplied with the LoRa baseband signal in digital domain. We try to integrate the de-chirping with down-conversion and passively achieve the two in analog domain to evade stressing the DBP. Multiplying real signals in analog domain will produce both upper sideband (USB, *i.e.*, sum frequency signal) and lower sideband (LSB, *i.e.*, difference frequency signal). If we still employ the base down-chirp for de-chirping, our desired resultant signal (after de-chirping) should be the USB. However, in this case, USB is still an RF signal which cannot be down-converted.

In Sisyphus, we instead employ the up-chirp for de-chirping. Thus the de-chirping operation will be performed in the LSB while down-conversion can be completed by the way.

Second, LoRa modulates its data through varying initial frequencies, which correspond to specific cyclical frequency shifting times within each chirp. We demodulate LoRa by localizing these times. However, the result after de-chirping is an envelope-constant signal with two segments of different frequencies due to the cyclical frequency shifting of LoRa. Directly detecting the frequency jump between the two segments requires bulky operations consuming quite a lot energy, which deviates from our original intent. In Sisyphus, we convert the jump detection from frequency into amplitude using passive, cheap and customizable RC filter. This allows us to demodulate LoRa using passive or ultra-low-power components such as rectifier and comparator.

Third, if we employ an unchanging base up-chirp for the de-chirping of LoRa, the relationship between the two frequencies within the LoRa chirp will change with LoRa chirp's initial frequency. For instance, if one chirp's initial frequency is less than 0, the frequency of the second segment will be higher than that of the first segment. But it would be the opposite when the initial frequency exceeds 0. So we cannot decide whether to use a low-pass filter (LPF) or a high-pass one. Moreover, the difference between the two frequencies is usually not large enough to be distinguished by filter, resulting in a minor difference between the amplitudes of the two segments after frequency-amplitude conversion. In Sisyphus, we modulate the helper signal into a base up-chirp with the same initial frequency as the equivalent LoRa chirp. The frequency of resultant signal's first segment will be 0 and the second segment's will be equal to the LoRa's bandwidth. The relationship between the two frequencies can be fixed and the difference is enlarged to a constant equals bandwidth, enabling the RF pattern more identifiable and robust.

To summarize, our contributions are three-fold:
- We propose a passive LoRa receiver with de-chirping capability, which can significantly prolong the battery life of LoRa devices and reduce maintenance costs in around-the-clock mode.
- We build a prototype system for proof-of-concept. We provide a solution to enable Sisyphus to be backward compatible with COTS LoRa infrastructure.
- Comprehensive experimental results demonstrate that printed circuit board (PCB) implemented Sisyphus achieves a remarkably low power of 162.7 μW in continuous operation mode with a line-of-sight (LOS) communication range of 73 meters. Incorporating the μW-level IF amplifier extends the LOS range to 107 meters, while significantly improving non-line-of-sight (NLOS) performance. Moreover, Sisyphus's robust interference immunity is also highlighted.
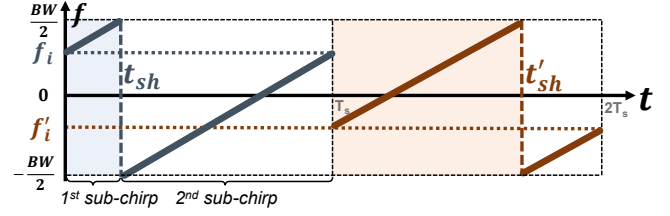
Figure 2: CSS modulation scheme adopted by LoRa. The initial frequency of each chirp corresponds to a specific cyclical frequency shifting time.

2 PRELIMINARY

This section first provides a primer on LoRa's modulation scheme. Then, the problem of legacy de-chirping of LoRa is articulated.

2.1 LoRa Primer

The modulation scheme of LoRa is shown in Figure 2. LoRa adopts a prominent CSS modulation, which modulates data bits using a linear varying frequency over time with different initial frequencies. The base up-chirp in baseband can be mathematically denoted by

$$c(t; f_i) = cos\left[2\pi(f_i + \frac{1}{2}kt - \frac{BW}{2})t\right], \ 0 \le t < T_s, \quad (1)$$

where f_i is the initial frequency of the chirp, k is the frequency changing rate (*a.k.a.*, the frequency modulation (FM) slope of chirp), BW as the bandwidth of LoRa chirp and T_s is the chirp symbol duration.

We can see from Figure 2 that when frequency grows to BW/2, the rest segment of LoRa chirp will perform frequency shift to -BW/2 and continue increasing with the same slope as before until the end of chirp symbol duration. Hence the LoRa chirp $s(t; f_i)$ can be expressed as

$$s(t; f_i) = c(t; f_i) \cdot w[t; 0, t_{sh}] + c(t; f_i - BW) \cdot w(t; t_{sh}, T_s), \ (2)$$

where t_{sh} is **cyclical frequency shifting time** within a LoRa chirp, which occurs when the chirp frequency exceeds BW/2. $f_i = i \cdot \frac{BW}{2^{SF}} - \frac{BW}{2}$ (i is the embedded value and SF denotes the spreading factor) is the specific initial frequency of LoRa chirp, $c(\cdot)$ is base up-chirp within the LoRa chirp, $w(t; a, b)$ is rectangular window function, which can be denoted as $w(t; a, b) = (a \le t < b) ? 1 : 0$.

2.2 Problem of Legacy LoRa's De-chirping

The CSS modulation employed by LoRa endows it with exceptional immunity to interference and an extended communication range by distributing its embedded information across the entire baseband spectrum. To harness the processing gain offered by this spread spectrum technology, LoRa receiver must perform de-chirping of the CSS-modulated
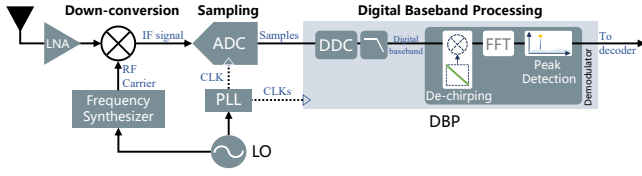
Figure 3: Diagram of legacy LoRa receiver.

Figure 4: Passive LoRa dc^2. The resultant signals are shown in both time and frequency domains.

signal. In legacy LoRa receiver, as illustrated in Figure 3, LoRa signal undergoes initial mixing with an ultra-high frequency (UHF) carrier generated by LO and PLL to conduct down-conversion. Subsequently, the signal is sampled by a power-intensive ADC and subjected to further DDC. The resultant digital baseband signal is then multiplied by a down-chirp signal generated by a numerically controlled oscillator (NCO), yielding a single-tone output. Simultaneously, the energy of any single-tone interference is diffused by the local down-chirp to a low enough strength that it won't distort the LoRa signal.

However, this de-chirping procedure requires power-hungry components, which typically consume tens of mW power, obviously infeasible for our long-term and around-the-clock expectation. Furthermore, it entails a laborious synchronization burden involving a computationally intensive correlation procedure. Therefore, to retain the processing gain of LoRa on Sisyphus, it is imperative to devise a de-chirping methodology with minimal overhead.

3 TIME LOCALIZATION DEMODULATION

In our scheme, we propose to convert the power-hungry legacy LoRa demodulation method, which relies on initial-frequency tracking, into cyclical frequency shifting time localization. The pivot of our demodulation method is to get the value of t_{sh} in each chirp, since

$$t_{sh} = \frac{\frac{BW}{2} - f_i}{k} = \frac{\frac{BW}{2} - (i \cdot \frac{BW}{2^{SF}} - \frac{BW}{2})}{\frac{BW^2}{2^{SF}}} = \frac{2^{SF} - i}{BW}. \quad (3)$$

We refer to the segment within the LoRa chirp before t_{sh} as the 1st sub-chirp, and the segment after t_{sh} within the chirp is called the 2nd sub-chirp. As shown in equation (3), as the SF and BW are given, we can obtain the value i carried by the first chirp easily by detecting t_{sh}. In other words, we can extract the data by calculating duty cycle of the 1st sub-chirp in each LoRa chirp, as depicted in the color-filled blocks of Figure 2. This scheme holds because LoRa waveform has a strong time-frequency correlation in nature due to its geometric feature.

4 PASSIVE LORA DC^2

The frequency shifting time localization based demodulation method enables the possibility of avoiding the existing
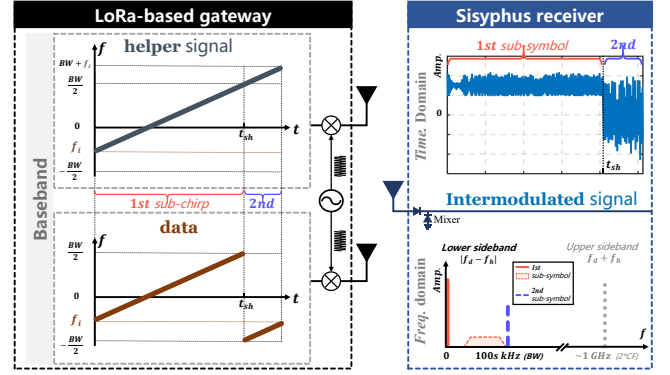
power-intensive components on legacy receiver. However, implementing it under power-constrained conditions is non-trivial. In this section, we will elaborate on our passive dc^2 methodology, including the signal model and analysis of resultant signals.

4.1 Signal Model

We leverage the abundant computation resource of LoRa-based gateway to generate our designed *helper* signal, as shown in Figure 4. Particularly, *helper* is a base up-chirp with the same slope k as the LoRa signal to be demodulated (we refer to it as *data* signal). However, its initial frequency is no longer $-\frac{BW}{2}$ but f_i, the same as *data*. The FM slope is controlled by SF and BW of *helper*, for $k = BW^2/2^{SF}$. The timing of *helper* is synchronized with *data*, which is easy to achieve on the LoRa-based gateway. We refer to frequency functions over time of *data* and *helper* as $f_d(t)$ and $f_h(t)$ respectively, for $0 \le t < T_s$, and we have

$$\begin{cases} f_d(t) = mod(f_i^d + kt, BW) - \dfrac{BW}{2}, \\ f_h(t) = f_i^h + kt - \dfrac{BW}{2}. \end{cases} \quad (4)$$

The two types signals delivered can be further denoted uniformly as

$$s_{type}(t) = a_{type} \times cos\left[2\pi\left(\int_0^t f_{type}(t)dt\right)\right], \quad (5)$$

where *type* includes d (refers to *data* signal) and h (refers to *helper* signal), and a_{type} is the corresponding amplitude for the two types of signals.

4.2 Intermodulation in Sisyphus

We up-convert both *data* and *helper* signals individually with the same RF carrier and transmit them from the transmitter (Tx) into the air. As the two signals propagate through

the air and encounter the diode-based passive mixer, intermodulation will be created [18, 19] due to the non-linearity of Schottky diode. Here, we establish the mathematical feasibility of our proposed LoRa dc^2 methodology. First, the non-linear function $\mathscr{F}(\mathcal{S})$ can be expressed in the Taylor series [20] as

$$\mathscr{F}(\mathcal{S}) = k_0 + k_1\mathcal{S} + + k_2\mathcal{S}^2 + k_3\mathcal{S}^3 + \cdots, \quad (6)$$

where k_n is the linear coefficient related to the linear gain of non-linear element. Given that the energy levels of resultant high-order harmonics are significantly lower than those of the first two orders, we opt to disregard them in this proof. When *data* signal $s_d(t)$ and *helper* signal $s_h(t)$ are injected into the non-linear system (*i.e.*, $\mathcal{S} = s_d(t) + s_h(t)$), we have

$$k_0 + k_1\left[s_d(t) + s_h(t)\right] + + k_2\left[s_d(t) + s_h(t)\right]^2. \quad (7)$$

Despite the fact that frequencies of chirp signals are varying at all time, for a given time t_0, the frequency function $f_{type}(t)$ in Eq. 5 is a constant. We let f_{d,t_0} and f_{h,t_0} denote the frequency value of *data* and *helper* at t_0. Hence, $s_d(t)$ and $s_h(t)$ can be approximated as a single-tone sinusoidal signal at t_0 with corresponding constant frequency f_{d,t_0} and f_{h,t_0}, namely $s_d(t) = a_d \times \cos\left(2\pi f_{d,t_0}t\right)$ and $s_h(t) = a_h \times \cos\left(2\pi f_{h,t_0}t\right)$. Then substituting them into Eq. (7), omitting the coefficients for formula simplicity and applying *double angle* formula and *prosthaphaeresis* formula, we get

$$\cos\left(2\pi f_{d,t_0}t\right) + \cos\left(2\pi f_{h,t_0}t\right) + 1 + \frac{1}{2}\cos\left(2\pi(2f_{d,t_0})t\right) +$$
$$\frac{1}{2}\cos\left(2\pi(2f_{h,t_0})t\right) + \frac{1}{2}\cos\left(2\pi(f_{h,t_0} + f_{d,t_0})t\right) +$$
$$\frac{1}{2}\underbrace{\cos\left(2\pi(\underline{f_{h,t_0} - f_{d,t_0}})t\right)}_{Expected\ harmonic}. \quad (8)$$

As shown in Eq. 8, apart from the fundamental, the frequency components of intermodulation occurring at t_0 mainly include the sum and difference of $s_d(t)$ and $s_h(t)$, which are the main upper sideband (USB) and lower sideband (LSB) signals, with frequencies of $f_{d,t_0} + f_{h,t_0}$ and $f_{h,t_0} - f_{d,t_0}$. We utilize the LSB of $f_{h,t_0} - f_{d,t_0}$, i.e., the last term in Eq. 8, to get dc^2 results. The proof outlined above establishes the validity of our argument for all discrete times within the duration of the two chirp signals. Moreover, in accordance with the Limit Theorem, chirp signals in analog domain also conform to this proof. As a result, we get the theoretical model of intermodulation on chirp signals.

Next we'll delve into the intricacies of passive LoRa dc^2 in detail. Our analysis initiates by analyzing the resultant LSB of both the 1st and 2nd sub-symbols' baseband, as well as the
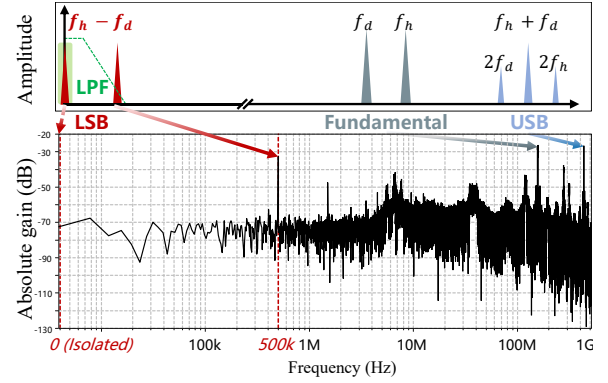
Figure 5: Spectrum of intermodulation in our work. DC components have been isolated by signal analyzer.

outcome of de-chirp processing. Subsequently, we will examine the results of RF portion in both the LSB and USB, elucidating the mechanics behind the passive down-conversion achievable through our solution. To enhance comprehension, we employ a CXA signal analyzer [21] to plot the spectrum of dc^2 outcomes from beating signals with pre-configured SF (7), bandwidth (500kHz) and carrier frequency (433MHz), as depicted in Figure 5.

The resultant LSB of the 1*st* **sub-symbol's baseband.** As mentioned earlier, the 1*st* sub-chirp of *data* and the 1*st* sub-chirp of *helper* are identical in their duration. After their passing through the diode mixer on the receiver altogether, a direct current (DC) signal in resultant LSB will be created, as plotted in Figure 4, owing to

$$f_h(t) - f_d(t) = 0, \forall\ t \in \{1st\ sub-chirp\}, \quad (9)$$

substitute Eq. (9) into Eq. (8), and we observe that the resultant LSB transforms into a zero-frequency signal with some other harmonic frequencies, precisely a DC-biased signal. Typically, intermodulation arises when two signals with disparate frequencies interact. However, in our scenario, where identical signals are introduced into the diode, the outcome illustrates that non-linear behavior can also manifest with identical signals.

The resultant baseband of the 2*nd* **sub-symbol.** As for the 2*nd* sub-chirps of *data* and *helper*, since the intrinsic geometric feature of LoRa chirps, the frequency difference $\Delta f = f_h - f_d$ between the two sub-chirps remains constant and is equal to BW, as shown in Figure 4. This is to say, when the two 2*nd* sub-chirps are fed into the diode mixer, a single-tone alternating current (AC) signal with a frequency of BW in the LSB is produced. As plotted in Figure 5, the 500kHz component we highlight is just the resultant LSB with our pre-configured 500kHz BW.
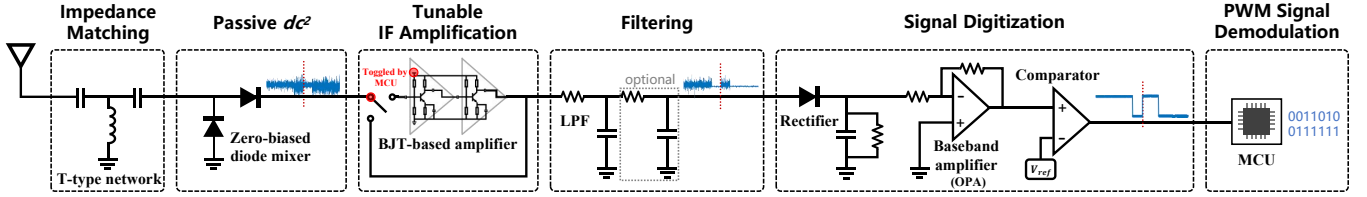
Figure 6: Low-power circuit design. Sisyphus employ the LPF for passive frequency-to-amplitude conversion.

The RF portion results in the resultant signal. After analyzing the LSB in terms of the two sub-symbols' baseband, let's move on to the RF portion in both LSB and USB on an entire symbol scale. Recalling that *data* and *helper* are multiplied by carriers for up-conversion before being delivered from Tx, and the carrier frequency (CF) is set to one of 433, 868 and 915 MHz, the resultant USB (whose frequency is equal to 2×CF) will be around 1 GHz, as shown in Figure 5. This USB can be eliminated easily by using a passive RC LPF. On the other hand, the carriers of up-converted *data* and *helper* are generated by the sharing oscillator (OSC) and the same configured PLL on the Tx side. As a consequence, carriers can be canceled in LSB (first converted into a DC component, and isolated by subsequent capacitors), thus achieving the passive down-conversion.

Thus, the resultant IF signal after intermodulation can be seen in Figure 4, where the $1st$ and $2nd$ sub-chirps within each chirp are effectively distinguished, accurately reflecting the duty-cycles of the sub-chirps within a LoRa chirp. This signifies the successful capture of the time-frequency characteristics of the original LoRa chirp. The residual weak harmonics can be removed by LPF, and the configure consideration of LPF will be stated in §5. Given the synchronized transmissions between *data* and *helper*, coupled with the instantaneous superposition property of wireless channels, our methodology ensures a seamless, delay-free transition between the $1st$ and $2nd$ sub-symbols. This guarantees highly reliable subsequent duty-cycle calculation. At this stage, we have accomplished one-shot dc^2 of the LoRa signal with zero on-device energy consumption.

5 LOW-POWER CIRCUIT DESIGN

Passive dc^2 has completed the down-conversion and de-chirping of LoRa. Next, we'll introduce our design of a low-power circuit for hardware supporting of demodulation, as sketched in Figure 6.

Passive frequency-to-amplitude conversion. We employ the RC LPF for the frequency-to-amplitude conversion. Firstly, we analyze what frequency components need to be filtered out in conjunction with Figure 5. The frequency of the USB in intermodulated signal is up to GHz level, which is

located far away from the expected signal and can be eliminated easily. In the LSB, the post-dc^2 $1st$ sub-chirp (hereafter referred to as sub-symbol), which is primarily a DC signal. And the frequency of the post-dc^2 $2nd$ sub-symbol reaches BW. Thus, we can not only pick up the desired LSB on symbol scale but also suppress the amplitude of the $2nd$ sub-symbol within the symbol of picked LSB by using a simple RC LPF and carefully setting its -3dB cutoff frequency.

Signal digitization. Subsequently, a rectifier is employed to rectify the filtered signal to obtain the converted amplitude. Here the resistor is employed to regulate the discharge rate of the capacitor in the rectifier, ensuring that the rectified signal accurately tracks the amplitude of the input signal. Then, we can amplify the baseband signal using a low gain–bandwidth (GBW) OPA with ultra-low power consumption. After feeding the amplified signal into the comparator, we can obtain the wave-shaped digital pulse width modulation (PWM) output with specific duty-cycles corresponding to initial frequencies of LoRa chirps, which allows us to perform data bit extraction by demodulating this PWM signal.

PWM demodulation. Finally, we calculate the duty-cycle of each PWM symbol using microcontroller unit (MCU) to achieve the data bit extraction. We first perform detection on signal edges and then record these rising/falling edges' times. Specifically, when edges coming, an according interrupt is fired and the value of Timer will be captured to a specific register. By calculating the time difference between the rising and falling time, we can obtain the duty-cycle of PWM symbol, which carries the data bits we long for. Here we use the low-power timer (LPTIM) to analyze the digital PWM signal output by comparator, which allows MCU to perform PWM demodulation in its Stop2 mode without the need for wake-up, rather than activating the energy-heavy multi-bit ADC peripheral. The comparator, can also be considered a 1-bit ADC, but with a current consumption of only $10\mu A$.

Tunable IF amplifier. We employ a two-stage common-emitter IF amplifier based on BJTs after the diode mixer to enhance the link budget of Sisyphus. Thanks to the low-frequency nature of the target components to be amplified,

we can achieve considerable gain with low energy consumption. Similar to the design in MIXIQ [16], to avoid the transistor entering the saturation region and causing signal distortion, we do not leave the amplifier running all the time. We employ an RF single-pole, double-throw (SPDT) switch as the bypass switch to activate/disable the IF amplifier. The Switch Select signal of SPDT, S_{sel}, is toggled by MCU. It also connects the GATE of a switch nMOS to control the power supply of BJTs. When we decide to activate the IF amplifier, we toggle S_{sel} as HIGH, according to the Truth Table of SPDT, the switch will throw to IF amplifier. At the same time, the SOURCE and DRAIN of nMOS conduct and Vcc starts powering the IF amplifier. On the contrary, when we want to disable the IF amplifier, we toggle S_{sel} as LOW. With this approach, we can achieve tunable IF amplification with convenience. It's noteworthy that the impedance of this BJT-based amplifier and the input resistance of the subsequent active component (*i.e.*, OPA) is both high, plus that the overall impedance of the line shown in Figure 6 is relatively high so that the current is small, which will not impact the subsequent RC filter. Therefore, we don't need to place a buffer between the IF amplifier and LPF/OPA. In addition, the BJT-based amplifier can only work on AC signal, however, as we discussed in §4, our 1*st* sub-symbol of intermodulated signal is primarily a DC signal, which will be seriously insulated by the capacitor in IF amplifier. In order to let the BJT-based amplifier properly operate on our intermodulated signal, we slightly modify *helper* when the IF amplifier is activated. Specifically, instead of employing the same initial frequency as *data*, we apply a little shifting on *helper*'s initial frequency than *data*. The receiver-side activation of IF amplifier is kept in step with the accordingly Tx-side signal modification. Thus, the 1*st* sub-symbol of the resultant signal becomes a low-frequency AC signal that can be amplified by IF amplifier. Additionally, for the non-linear distortion concern of BJTs, in fact, the BJT can properly work in its linear region for the vast majority of cases. To prepare for any eventualities, we have still fine-tuned the v_{BE} (voltage falling between the base and emitter of BJT) and v_{CE} (voltage falling between the collector and emitter of BJT) to ensure BJTs to work at the linear region.

6 BENEFIT ANALYSIS OF PASSIVE DC^2

In this section, we will exhibit the benefit of our passive dc^2 methodology. Firstly, we proof the maintenance of LoRa's channel concurrency. By the same token, we also exhibit its interference immunity for both single-tone and spread spectrum signals.

Channel concurrency. LoRa supports concurrent transmissions from orthogonal channels, where chirps have different slopes (slope $k = BW^2/2^{SF}$). This is because when
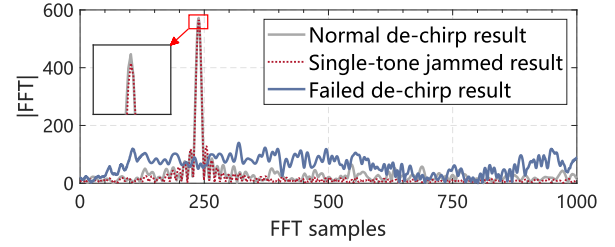
Figure 7: FFT results after the normal, single-tone jammed and failed de-chirping.

conducting a dc^2 operation, the expected single-tone signal shown in the gray curve of Figure 7 can appear only when $|k|$ of LoRa chirp and base down-chirp is the same. We'll describe the mathematical model of why our passive dc^2 can also ensure the original concurrency of LoRa. For formula simplification, we denote the intermodulated signal as

$$\sum_{m=-\infty}^{+\infty} \sum_{n=-\infty}^{+\infty} \alpha_{mn} cos \left\{ 2\pi \left[m(f_i^1 + k_1 t) + n(f_i^2 + k_2 t) \right] t \right\}.$$

When two chirps with different $|k|$ are fed into the passive dc^2 model, the frequency of intermodulated signal is $m(f_i^1 + k_1 t) \pm n(f_i^2 + k_2 t)$. We cannot get the expected LSB with a frequency of $f_i^1 - f_i^2$ if $k_1 \neq k_2$. The dc^2 operation will fail and the FFT result of the failed post-dc^2 signal is shown in the blue curve of Figure 7. We can see that the resultant signal is still a spread-spectrum signal. As §5 described, the onboard LPF's cutoff frequency is set to only allow the 1*st* sub-symbols' LSB (mainly DC) to pass through. In other words, chirps with different $|k|$ than *helper* can be separated by our scheme. Thus, our scheme ensures the original concurrent channels presented in the LoRa specification.

Interference immunity. By means of the same proof approach, when a single-tone signal with the frequency of f_{sin} enters the diode mixer with LoRa signal, we get the resultant frequency of $m(f_i + kt) \pm n f_{sin}$. This indicates that the single-tone interference signal is spread across the spectrum, which cannot pass through the on-board LPF. We're still able to demodulate the target LoRa signal with the single-tone interference, as plotted in the dotted red curve in Figure 7. Moreover, a spread spectrum signal with the different $|k|$ than *helper* cannot pass through the onboard LPF either, as we described above. Therefore, our passive LoRa dc^2 has a similar anti-interference effect as its active counterpart, obtaining the processing gain of CSS as well.

7 START FRAME DELIMITATION

MCU performing data extraction needs to know where the payload starts in a LoRa packet. Legacy LoRa relies on digital de-chirping to search the start frame delimiter (SFD) within
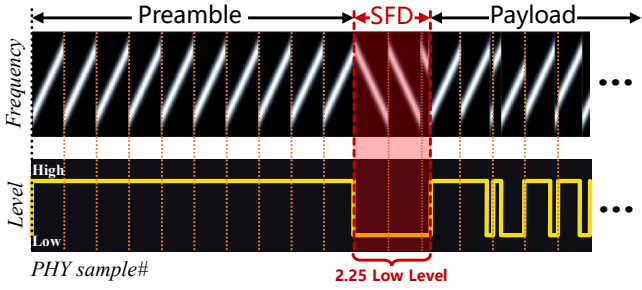
Figure 8: Start frame delimitation in Sisyphus. We indicate the start of the payload by detecting the 2.25 low level output from the comparator.

Figure 9: Prototype of Sisyphus hardware and equipments employed in our experiment.

the LoRa packet, a distinctive 2.25 down-chirp highlighted in Figure 8. In Sisyphus, the SFD equivalent *helper* is specifically designed to be 2.25 down chirps, shifted by *BW* relative to the SFD frequency. All the frequency components in the SFD's resultant signal after passive dc^2 will be much higher than the cutoff frequency of LPF, which cannot pass through it. The SFD's resultant signal before its input to MCU is a continuous low level with a duration of 2.25 symbols. Thus MCU can perform start frame delimitation by measuring the duration of this low level. Specifically, MCU stays in the low-level duration measurement mode until it detects a 2-symbol-duration low level (the remaining 0.25 symbol durations are reserved for level duration measurement mode switching.). After this, the MCU turns into the high-level duration measurement mode to perform data extraction on the payload. Consecutive 2.25-low-level cannot occur in the payload, thus it can distinctly indicate the payload's start.

8 IMPLEMENTATION

Figure 9 shows the 3.7cm × 2.4cm four-layer FR4 PCB prototype of Sisyphus's hardware and the equipment we employed in our evaluation. We describe the hardware and software implementation of the Sisyphus prototype as follows.

LoRa-based gateway for transmission: We use NI USRP 2944 with 6dBi gain antennas as the Tx in early development for convenience. We fabricate the digital *helper* on PC and transmit it using USRP along with *data* synchronously. Whereas in later research, for backward compatibility with legacy LoRa, we employ the commercial off-the-shelf (COTS) LoRa module for *data* and *helper* delivery. The realization detail can be seen in §9.5.

Matching network and diode mixer for passive dc^2: We use two capacitors and one inductor to form a T-type impedance matching network. We adjust their value to make the *S11* parameter (measured by a vector network analyzer (VNA) [22]) lower than -20*dB* in the frequency band of 914-917MHz. Moreover, we also reproduce this procedure on
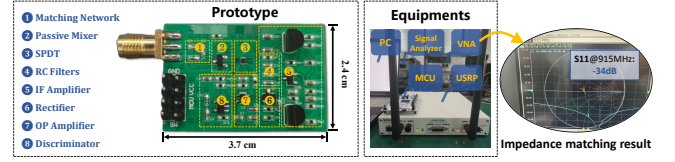
other two prototypes in the frequency bands of 866-869MHz and 431-434MHz for our follow-up experiment. We employ SMS7630-005LF RF diodes [23] as the mixer for passive dc^2, which has a decent conversion gain.

RC low pass filters: We empirically initialize the -3dB cutoff frequency of LPF to 1.3 kHz and in practical deployment, we adjust it to optimize the communication performance.

Signal digitization and data bit extraction: We let MAX9914 [24] serve as the OPA, draining 51.7 μW for 8 dB sensitivity gain. And we use NCS2200 [25] as the comparator, which consumes only 17.6 μW. In addition, we employ STM32U5 [26] to perform the data bit extraction from PWM signal, which is an ultra-low-power MCU with low-power background autonomous mode (LPBAM).

IF amplifier: The IF amplifier is implemented by BJTs, served by Onsemi 2N3904 [27] with 300 MHz characteristic frequency, powered by 1.8V and biased by large resisters. And the two stages of amplification circuit is coupled by capacitors. We employ HMC536 [28] for the SPDT switch and DMG2302 [29] is used for the switch nMOS.

9 EVALUATION

To evaluate the intrinsic performance of passive dc^2, we distinguish the version with the IF amplifier activated as Sisyphus+. As for the communication evaluation, we let the Tx send 5,000 packets total, and each packet contains 64 encoded symbols within its payload. Unless specified otherwise, BW, CF and SF are set to 125 kHz, 433 MHz and 7. After demodulation, the PC undertakes the decoding offline using an open-source LoRa physical layer tool [30]. The gain of receiver's antenna is 3dBi.

9.1 Power Breakdown

We analyze the power of Sisyphus (1.8V supply) and legacy LoRa module (EBYTE E32T20S [31] with 3.3V supply) using a DC power analyzer [32] and compare them to 6 other benchmarks, which are described below. The comparison result is illustrated in Figure 10.

Saiyan [13]: the most related work with Sisyphus. We find that its power can be up to 430mW from the bill-of-materials (BOM) of the project link provided in their paper. Such power
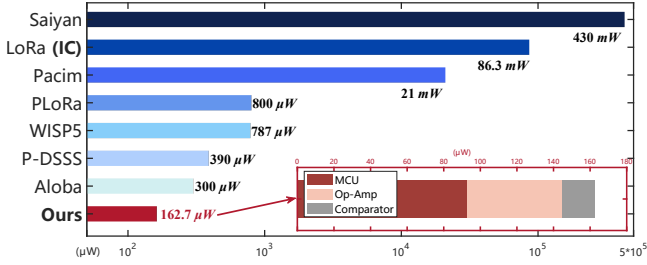
Figure 10: Power comparison between Sisyphus and benchmarks. PCB-implemented Sisyphus achieves 530× power savings compared to IC-implemented legacy LoRa.

(a) Sisyphus.

(b) Sisyphus+.

Figure 11: Receiving sensitivity.

is mainly originated from its used LNA (TQP3M9008 [14]) and IF amplifier (OPA810 [15]).

PLoRa [11], Aloba [8] and Pacim [10]: three typical LoRa backscatter systems, the former two follow the envelope detector (ED)-ADC-DBP architecture for their downlink and the last employs a mW-level COTS energy detector chip [33]. All of them have no LoRa demodulation ability but can only perform signal detection.

Passive DSSS [34]: an ED-based receiver with low-power de-spreading of on-off keying (OOK) modulated direct sequence spread spectrum (DSSS) signals. Its power is predominantly occupied by OPA [35], DBP and comparators.

WISP5 [36]: a popular computational radio frequency identification (CRFID) system with a downlink receiver that includes an ED, comparator and DBP.

The power of each component in Sisyphus is plotted as well, which is made up of MCU, OPA, and comparator, while all other components consume zero power. Benefiting from the LPBAM implemented by MCU's hardware subsystem, its power can be as low as 93μW, which is still the major source of Sisyphus's total power. This part can be reduced dramatically when implemented with an integrated circuit (IC). We can see that PCB-implemented Sisyphus consumes 162.7μW in total, 530× reduction compared to legacy LoRa receiver, and 2643× reduction compared to Saiyan. In contrast to PLoRa, Aloba and Pacim, which have no symbol-level demodulation ability, Sisyphus still has 4.9×, 1.8×, and 129× power savings. When the IF amplifier is activated, it contributes around 286μW to the overall power consumption.

It's also noteworthy that the power of LoRa we compared is the result of our actual measurement. The reason why this result is much higher than that of Semtech's datasheet is that they only list the single chip's power. Whereas the practical form factor of a legacy LoRa receiver is an RF module with a set of off-chip components, which introduce quite a bit of energy drain. In addition, the power of LoRa receiver we compare is that of the IC version. We also conduct a modular
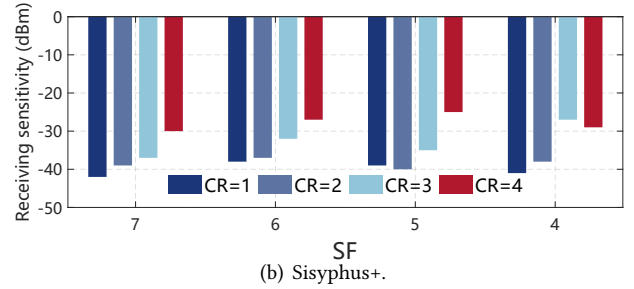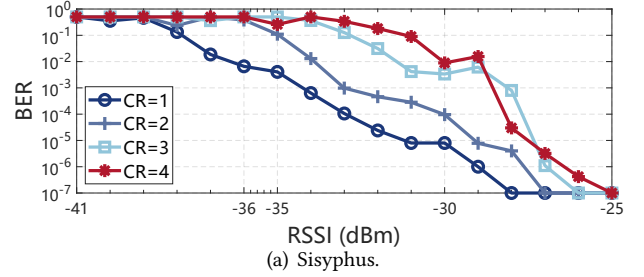
analysis of CMOS simulation for each active block of Sisyphus. We employ TSMC 65nm CMOS technology to build a baseband amplifier (*i.e.*, OPA) with 100kHz GBW and the comparator, draining 7.4 μW and 0.8 μW with 0.8V supply respectively. For the most power-consuming part left, the digital part, we use Synopsys DC for power simulation of the register transfer level (RTL) design of PWM demodulation and the result shows that the digital part consumes 8.5 μW with 1.8V supply. The overall power consumption of Sisyphus stands at 16.7 μW. When powered by a 1500mAh AA battery, the battery life can be extended to more than 10 years in around-the-clock operation mode.

9.2 Receiving Sensitivity

Receiving sensitivity directly affects the communication performance of the receiver. We evaluate the receiving sensitivity by testing the bit error rate (BER) of Sisyphus with received signal strength indicator (RSSI) and coding rate (CR) changing in our laboratory. To facilitate the RSSI control, we use one RF chain to deliver *data* and *helper*. We connect the TX (USRP) and the receiver using an RF cable and incorporate several RF attenuators within the cable. Then we adjust the signal strength and the number of attenuators according to our wanted RSSI. For accurate RSSI control, we calibrate the signal power using the CXA signal analyzer [21]. The extracted data bits will be forwarded by MCU to PC for BER analysis. When BER is becoming lower than 1 %, we record the RSSI then as the receiving sensitivity.

9.2.1 Sisyphus. In this evaluation, we switch off the IF amplifier. We can see from Figure 11(a) that the best receiving
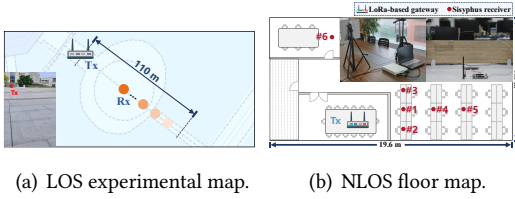
(a) LOS experimental map.

(b) NLOS floor map.

Figure 12: Experimental map.

(a) LOS demodulation range (outdoor).

(b) NLOS BER (indoor).

Figure 13: LOS and NLOS evaluation results.

sensitivity of Sisyphus is -36dBm when CR = 1. It's worth noting that since DR = SF×(BW/2^{SF})×CR, the theoretical data rate (DR) when CR = 1 reaches around 7 kbps [2], which is still the lowest in this experiment setup. If we further reduce DR to sub 1kbps, we may get better sensitivity. Additionally, we can find that BER increases when CR is tuned from 1 to 2, however, when tuned from 3 to 4, BER doesn't exactly fit the previous pattern. This is probably because a higher CR means a higher DR and therefore a higher BER, whereas on the other hand, a higher CR means more bits are used for forward error correction (FEC) and a stronger anti-interference ability. Here, the anti-interference effect brought by CR is probably more significant than the negative effect brought by the increasing DR.

9.2.2 Sisyphus+. We activate the IF amplifier and obtain the receiving sensitivity of Sisyphus+ when SF = 5, 6, 7. The frequency response is adjusted to the frequency of LSB (*i.e.*, hundreds of kHz). Figure 11(b) plots the experimental result, from where we can see that the receiving sensitivity will be enhanced to -42dBm when SF and CR are set to 7 and 1. The theoretical range can be reached up to 190 meters [37] with 23dBm transmission power. The experimental results show that the IF amplifier we implemented can bring a 6dB gain to our system.

9.3 Real-world End-to-end Evaluation

We evaluate the real-world communication performance of Sisyphus and Sisyphus+ in both LOS and non-LOS (NLOS) scenarios. In this evaluation, we use two RF chains on USRP 2944, transmitting *data* and *helper* at a transmission power of 20dBm (which is available by most COTS LoRa infrastructures) respectively. Since PLoRa, Aloba, and Pacim cannot demodulate LoRa signals, and Saiyan employs the LNA and OPA consuming three orders of magnitude more power than Sisyphus, we choose WISP5 as the benchmark in this evaluation. And its antenna gain and transmission power are configured the same as Sisyphus.

9.3.1 LOS and NLOS communication evaluation. **1) LOS.** We gradually move the receivers away from the Tx. At each step, we record the bits after demodulation to obtain the BER. The
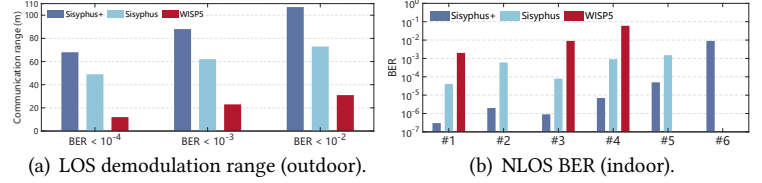
LOS evaluation is conducted on a campus street, as shown in Figure 12(a). We test Sisyphus and Sisyphus+ at fixed SF (7) and CR (1), indicating that DR is 6.8kbps. We set 3 BER thresholds (*i.e.*, BER<10^{-4}, BER<10^{-3} and BER<10^{-2}), and derive the according communication ranges. Figure 13(a) depicts the experimental results, showing that Sisyphus+ can achieve a 107-meter accurate demodulation at BER <10^{-2}. The communication range of Sisyphus can also reach over 70 meters, which is 2-4× compared to vanilla ED on WISP5 with similar energy consumption. Sisyphus+ trades 2.7× power for 1.5× range gain than Sisyphus, thus here Sisyphus may have a better price/performance ratio of power/range than Sisyphus+. **2) NLOS.** We also evaluate the NLOS wireless communication performance in the office shown in Figure 12(b). A pair of patch antennas with 12dBi is employed for this evaluation. We fix the Tx at the same location and place the receivers at 6 different locations of the office. Location #6 and the Tx are 2 walls away, and the others are 1 wall apart from the Tx. We can see from Figure 13(b) that the performance of Sisyphus+ is quite well at all 6 locations. Especially at location #6, it can demodulate the signals that penetrate 2 walls. However, the vanilla ED equipped on WISP5 can only work at location #1, #3 and #4. This evaluation demonstrates the great performance of Sisyphus+ in NLOS scenarios.

9.3.2 Goodput. Having discussed the sensitivity and communication performance in both LOS and NLOS, we now turn to look at the performance of Sisyphus's goodput. We define goodput here as the data bit rate of the delivered payload after decoding. So the goodput here is different from the DR (overall binary bit rate delivered) we mentioned above. We test how the goodput of Sisyphus varies with the DR by performing 30 evaluations at 6 locations (5 evaluations at each location) in the office, plotted in Figure 12(b). In our evaluation, we adjust CR when SF = 7, and BW = 500kHz. Figure 14 shows the cumulative distribution function (CDF) of 30 goodput results, from where we can see that the goodput increases with CR decreasing. This inverse relationship is because the higher the CR, the more redundant bits are used for FEC, and the proportion of payload bits used for data embedding decreases. We can see that Sisyphus can support demodulation up to 19kbps in real-world testing. Therefore,
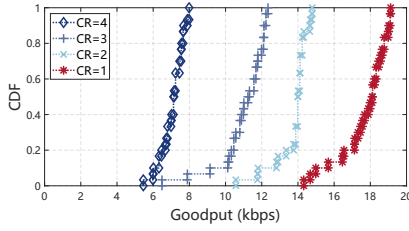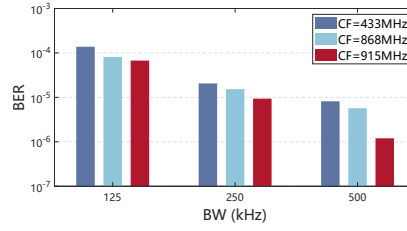
Figure 14: CDF of goodput.
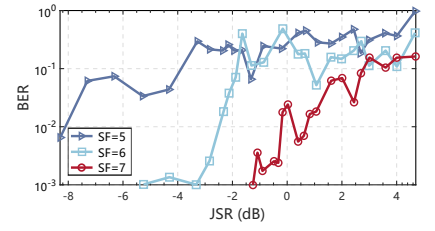

Figure 15: Impact of BW and CF.

Figure 16: Anti-jamming result.

with extremely limited resources, we have achieved a reasonably high level of communication efficiency.

9.3.3 The impact of RC filters. Our designed passive frequency-to-amplitude conversion approach's performance is based on the LPF's suppression effect of high-frequency components. So the impact of LPF cannot be trifled with. As we described before, the Δf of the 1*st* and 2*nd* sub-chirp within a LoRa chirp is decided by BW. The larger the BW, the larger the frequency interval between the two sub-symbols, and the more effective the LPF is in distinguishing between the two sub-symbols. This distinguishing degree has a considerable impact on the communication performance of Sisyphus. Additionally, the voltage drop of the mixer diode is impacted by frequencies. So we test how BER varies with BW and CF when RSSI = -30dBm, SF=7, CR = 1, and IF amplifier disabled, and one RF chain is used for cable transmission. We can observe from Figure 15 that BER decreases when BW increases. This is exactly since the larger BW means a better LPF suppression effect (for BW determines the Δf between helper and data signal) and a better effect of the spread spectrum. Therefore, we can get a more robust demodulation capability. Besides, in the sub-GHz level of our evaluation, the performance of Sisyphus gets better with increasing CF, which depends on the characteristics of the mixer diode used. In practical implementation, it is expected to set the -3dB cutoff frequency of LPF as low as possible, provided that the charging rate of capacitors within the LPF remains undistorted.

9.4 Interference Immunity Performance

In this section, we evaluate the real-world anti-interference performance of Sisyphus (here we term the interference as jamming, for it is deliberately performed). The IF amplifier will not boost the anti-jamming ability of Sisyphus as it also amplifies jamming, so we here disable the IF amplifier. We test the communication performance under single-tone jamming at SF = 5, 6, and 7, and we configure CF=915MHz, BW=500kHz. To avoid other unknown interference sources from misleading our experimental results, we add the single-tone jamming to the downlink signals (*data* and *helper*) beforehand and transmit them in one RF chain through an RF

cable with pretty anti-interference ability. We have carefully tuned the signal and interference strengths to accommodate different JSRs. Figure 16 plots the experimental results, which showcase that Sisyphus can achieve accurate communication (BER<10^{-2}) with positive JSR when SF=7, validating the theoretical discussion in §6.

9.5 Compatibility with COTS LoRa Module

This section will showcase the backward compatibility of our communication paradigm with the COTS LoRa module. Specifically, we build a helper emitter using a 433MHz COTS LoRa module [31], as shown in Figure 17.

Synchronization. When employing both LoRa device (data emitter) and helper emitter as the transmission infrastructure, synchronization between the two devices should be performed. Here, we use the common adopted reference signal for synchronization [38]. That is, one device sends a reference packet to another one, once the LoRa device listens to the start sign sent by helper emitter, it will convert to Tx mode right away and synchronizes its local time and carrier frequency accordingly. The processing delay incurred during this procedure remains largely consistent and can be precisely compensated for distinct communication parameters. Consequently, we are able to preemptively compensate for the transmission and reception delays by adjusting the transmission timing based on a preliminary estimation.

Creation strategy of *helper*. The *helper* is practically a base up-chirp, nothing but its initial frequency in baseband is not $-\frac{BW}{2}$ but f_i. Therefore, we can get *helper* by adding a delta frequency of $f_i - (-\frac{BW}{2})$ on each symbol of base up-chirps generated by COTS LoRa transceiver. Even though this operation is invalid in LoRa's baseband standard, we can still achieve the frequency shifting by directly modifying the RF, since the frequency of the up-converted signal equals the sum of baseband frequency and carrier frequency. Intuitively, we may mix the up-converted base up-chirp output by the COTS LoRa transceiver with the delta frequency to perform frequency shifting. However, since the employed delta frequency is less than BW the two resultant mirror copies will overlap with each other, we cannot use filters to pick up our desired USB. To address this, we find that
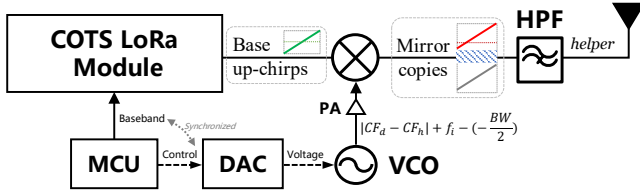
Figure 17: Creation of *helper* with COTS LoRa module. The power amplifier (PA) is employed to balance the input power between mixer's two ports.
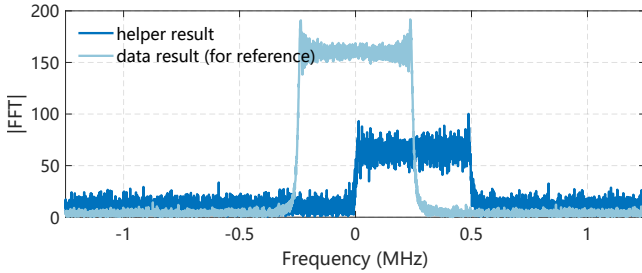
Figure 18: *helper* creation result. A helper signal is created from the base up-chirp output by a COTS module.

in Semtech SX127x series [2], CF can be programmed via register *RegFrf*, the relation is: $CF = F_{STEP} \times RegFrf(23:0)$, where F_{STEP} is the frequency step with the frequency of around 61 Hz. This allows us to assign a smaller CF for the COTS LoRa module within *helper* emitter than *data* emitter (LoRa device), *i.e.*, $CF_h < CF_d$. Therefore, the delta frequency of $|CF_d - CF_h| + f_i - (-\frac{BW}{2})$ will be much larger than BW, avoiding the overlap between mirror copies. We build a look-up table (LUT) of delta frequency by offline calculation from the above equation. We then use the MCU to manipulate the voltage controlled oscillator (VCO) based on the pre-established LUT through a digital-to-analog converter (DAC) to generate the corresponding delta frequency. The delta frequency generation and baseband output is performed synchronously. Finally, we can pick up the desired USB using a high-pass filter (HPF). The frequency jitter caused by imperfect hardware is very small, as low as 10Hz-level, while the symbol rate of LoRa is typically kHz-level, thereby the frequency jitter can hardly affect the communication. All the connectors between each components are SMA with impedance of 50Ω, avoiding the need for impedance matching.

Figure 18 plots the baseband results for *helper* signal created by our customized helper emitter and reference signal created by LoRa device. Hence, by performing such software-hardware co-design, the COTS LoRa module is competent for the creation of *helper*, thus validating the effectiveness of our effort on the integration.

10 RELATED WORK

At present, low-end IoT devices are becoming the mainstay of IoT markets. To drive their wider deployment, further reductions in cost and energy consumption are critical. There is a flurry of research on this. EkhoNet [39], R2B [40], and LEGO [41] propose to remove the redundancy of computation or chip control on end devices, significantly saving the power and fabrication cost. There are also tremendous works on ultra-low-power communication, including the downlink (receiver) and uplink (backscatter).

Low power receiver. According to their key optimization objective, we categorize them into: **i. Down-conversion:** The most common solution trying to break down the power of down-conversion is to exploit the diode mixer for passive down-conversion [16, 17, 42–47]. They leverage the external source for carrier generation. The difference between their solution and ours is: we perform passive dc^2 of LoRa in one shot while they can only down-convert the non-spread-spectrum signal to the single-tone lower frequency. In other words, their solution is futile for the popular spread-spectrum technologies; **ii. De-spreading:** To enhance the communication performance of low-end IoT devices, researchers devoted to ultra-low-power spread spectrum communication systems. Passive DSSS [34] achieves the passive de-spreading of DSSS signal by employing another channel to carry synchronized spreading code. But it can merely de-spread the vulnerable OOK modulated signal, leading to its limited gain compared to vanilla ED while consuming 3× power. And their RF link adheres to a 2Tx-2Rx architecture, where the two frequency-divided RF channels operate independently or in a quasi-orthogonal manner. Consequently, during communication, synchronization must be meticulously maintained between the two channels not only at Tx side but also Rx side, introducing substantial additional costs and complexity. Moreover, *μ*Mote [48] introduces a pair of twin up-chirps for passive chirp signal reception. Nevertheless, they can only de-spread the customized non-LoRa chirps, rather than LoRa-standard signal. And *μ*Mote carries only one bit data on every symbol in its waveform design, while Sisyphus can carry multi-bit data by relying on LoRa's PHY modulation scheme so that its bit energy budget is essentially lower than *μ*Mote. Particularly, Saiyan [13] is the most related work to ours. It uses the converted envelope for demodulation, without engaging in the de-spreading of LoRa. So it has no interference resilience capability, defeating the original purpose of implementing spread spectrum techniques. In contrast, our work enables passive de-spreading of LoRa, thereby maintaining pretty interference immunity.

LoRa backscatter systems. Benefiting from the ultra-low-power nature, backscatter communication is in the spotlight as one of the low-end IoT devices. However, most of

them suffer from extremely short range. There has been a large volume of recent works [8–12, 49, 50] on long-range backscatter communication. By introducing LoRa carrier into backscatter communication, they can obtain the processing gain of CSS and thereby longer uplink range. However, in contrast, applying LoRa demodulation on a downlink will involve much of an unaffordable energy budget. So they can only use the vanilla ED for packet-level detection on downlink. The highly efficient communication calls for symbol-level demodulation. Thus, an asymmetric plight arises between uplink and downlink communication. Sisyphus may break this tough obstacle by ultra-low-power symbol-level LoRa demodulation with passive dc^2.

Offloading in IoT systems. There are a range of works committing to offloading the most on-device power/cost-intensive components to the edge gateway, including but not limited to LO [8–12, 16, 17, 46, 48, 49, 51–58], storage [59], ADC [60] and processor [40, 61, 62]. Sisyphus shifts the tricky generation burden of carrier and signal for de-chirping to the existing gateways in the LoRa network.

11 DISCUSSION

In this paper, we provide a suitable solution for the sub-mW LoRa receiver. There are some concerns in our design, as discussed in the following.

Range compromise. Although Sisyphus seems to have a limited range in Figure 13(a), however, this is based on our power of no more than 400μW (PCB). Our contribution lies in passive dc^2, granting extra processing gain with no need for on-device energy, which provides us a better value for the money we pay. If we implement Sisyphus with an IC and add a low-power CMOS-based LNA [63] with 20dB gain, Sisyphus can communicate over 500m with no more than 1mW power. This represents a 100× power saving compared to legacy LoRa receivers, with a maximum 15× range compromise, which can be a trade-off and manually tunable.

Additional channel usage. We have demonstrated the feasibility of creating *helper* by applying software-hardware modification on the COTS LoRa module in §9.5. However, due to our used *helper* signal, the deployability of Sisyphus might still be challenged, for the possible employment of additional channel. This is a shared trait with backscatter-represented passive communication, and we're seemingly no exception. But in fact, when integrated into a backscatter device, Sisyphus not only enhances the downlink robustness but also confers a dual benefit by leveraging the existing base station infrastructure that the backscatter device inherently depends on, thereby mitigating the necessity for additional gadgets. And we believe that with the dramatic growth of LoRa, a substantial fraction of LoRa-based gateways can easily cope with multi-channel communication

[64–66]. Furthermore, we acknowledge that *helper* signal may affect non-Sisyphus LoRa communication that locates in the non-orthogonal channel (*i.e.*, has the same FM slope) with Sisyphus. To minimize this side effect, we hold that a carrier-sense multiple access (CSMA) protocol [67] can work for Sisyphus to avoid its collision with other non-Sisyphus communication.

Passive mixer. Passive dc^2 using Schottky diode based mixer will cause energy loss of received signal. Because we only utilize the LSB for demodulation and most of the other harmonics are filtered out. We incorporated a dual-diode mixer to mitigate this issue. We may employ a biased double-balanced mixer to cancel the fundamental for desired signal enhancement, but this will incur extra energy consumption. This is a trade-off problem.

Limited available SFs. Sisyphus keeps the SF below 8 when $BW \geq 125$kHz for robust communication, which is proportional to the varying step of PWM signals' duty-cycles (*i.e.*, chip duration of LoRa symbol, equals $\frac{1}{BW}$). The larger the varying step, the more duty-cycles we can distinguish. the larger SF can be applicable. So if we use a lower BW (official BW is 7.8kHz minimum), larger SFs can be applied to Sisyphus. On the other hand, as §9.3.3 demonstrated, lower BW may impair communication performance, whereas larger SFs in exchange can strengthen communication in some respects. There is a trade-off between larger SFs and lower BWs as well.

12 CONCLUSION

This paper proposes an ultra-low-power LoRa receiver called *Sisyphus*, designed for addressing the runtime energy consumption of LoRa receiver. Benefiting from our redesigned receiver architecture and passive dc^2 methodology, Sisyphus can achieve promising power savings of 27.2dB (530×) with its disadvantaged PCB prototype compared to legacy IC-implemented LoRa receiver. This power level is comparable to that of vanilla ED but offers at least 3× communication range. The experimental result also shows that Sisyphus can retain LoRa's anti-interference ability with zero energy consumption. Sisyphus is expected to pave the way for self-sustainable and around-the-clock operation of LoRa devices.

ACKNOWLEDGMENTS

REFERENCES

[1] Future Market Insights. Lora and lorawan iot market outlook from 2024 to 2034. https://www.futuremarketinsights.com/reports/lora-and-lorawan-iot-market, 2024.

[2] Semtech. SX1278. https://www.semtech.cn/products/wireless-rf/lora-connect/sx1278, 2024.

[3] Emiliano Sisinni, Abusayeed Saifullah, Song Han, Ulf Jennehag, and Mikael Gidlund. Industrial internet of things: Challenges, opportunities, and directions. *IEEE transactions on industrial informatics*, 14(11):4724–4734, 2018.

[4] Wenquan Liu, Xin Wang, Yongxin Song, Ruirui Cao, Liangliang Wang, Zhengguang Yan, and Guiye Shan. Self-powered forest fire alarm system based on impedance matching effect between triboelectric nanogenerator and thermosensitive sensor. *Nano Energy*, 73:104843, 2020.

[5] Zhaoxin Chang, Fusang Zhang, Jie Xiong, Junqi Ma, Beihong Jin, and Daqing Zhang. Sensor-free soil moisture sensing using lora signals. *Proceedings of the ACM on Interactive, Mobile, Wearable and Ubiquitous Technologies*, 6(2):1–27, 2022.

[6] Panasonic. Cr2032 coin-type lithium battery. https://industrial.panasonic.com/cdbs/www-data/pdf2/AAA4000/AAA4000C321.pdf, 2022.

[7] Yidong Ren, Puyu Cai, Jinyan Jiang, Jialuo Du, and Zhichao Cao. Prism: High-throughput lora backscatter with non-linear chirps. In *IEEE INFOCOM 2023-IEEE Conference on Computer Communications*, pages 1–10. IEEE, 2023.

[8] Xiuzhen Guo, Longfei Shangguan, Yuan He, Jia Zhang, Haotian Jiang, Awais Ahmad Siddiqi, and Yunhao Liu. Aloba: rethinking on-off keying modulation for ambient lora backscatter. In *Proceedings of the 18th Conference on Embedded Networked Sensor Systems*, pages 192–204, 2020.

[9] Jinyan Jiang, Zhenqiang Xu, Fan Dang, and Jiliang Wang. Long-range ambient lora backscatter with parallel decoding. In *Proceedings of the 27th Annual International Conference on Mobile Computing and Networking*, pages 684–696, 2021.

[10] Yuxiang Peng, Shiyue He, Yu Zhang, Zhiang Niu, Lixia Xiao, and Tao Jiang. Ambient lora backscatter system with chirp interval modulation. *IEEE Transactions on Wireless Communications*, 22(2):1328–1342, 2022.

[11] Yao Peng, Longfei Shangguan, Yue Hu, Yujie Qian, Xianshang Lin, Xiaojiang Chen, Dingyi Fang, and Kyle Jamieson. Plora: A passive long-range data network from ambient lora transmissions. In *Proceedings of the 2018 conference of the ACM special interest group on data communication*, pages 147–160, 2018.

[12] Vamsi Talla, Mehrdad Hessar, Bryce Kellogg, Ali Najafi, Joshua R Smith, and Shyamnath Gollakota. Lora backscatter: Enabling the vision of ubiquitous connectivity. *Proceedings of the ACM on interactive, mobile, wearable and ubiquitous technologies*, 1(3):1–24, 2017.

[13] Xiuzhen Guo, Longfei Shangguan, Yuan He, Nan Jing, Jiacheng Zhang, Haotian Jiang, and Yunhao Liu. Saiyan: Design and implementation of a low-power demodulator for {LoRa} backscatter systems. In *19th USENIX Symposium on Networked Systems Design and Implementation (NSDI 22)*, pages 437–451, 2022.

[14] Qorvo. Tqp3m9008. https://www.qorvo.com/products/p/TQP3M9008, 2023.

[15] Texas Instruments. Opa810. https://www.ti.com/product/OPA810, 2019.

[16] Mohammad Rostami, Xingda Chen, Yuda Feng, Karthikeyan Sundaresan, and Deepak Ganesan. Mixiq: re-thinking ultra-low power receiver design for next-generation on-body applications. In *Proceedings of the 27th Annual International Conference on Mobile Computing and Networking*, pages 364–377, 2021.

[17] Fengyuan Zhu, Luwei Feng, Meng Jin, Xiaohua Tian, Xinbing Wang, and Chenghu Zhou. Towards ultra-low power ofdma downlink demodulation. In *Proceedings of the 20th ACM Conference on Embedded Networked Sensor Systems*, pages 725–739, 2022.

[18] PL Lui. Passive intermodulation interference in communication systems. *Electronics & Communication Engineering Journal*, 2(3):109–118, 1990.

[19] Hugo Cravo Gomes and Nuno Borges Carvalho. The use of intermodulation distortion for the design of passive rfid. In *2007 European Radar Conference*, pages 377–380. IEEE, 2007.

[20] Noureddine Boulejfen, Afef Harguem, and FA Ghannouchi. New closed-form expressions for the prediction of multitone intermodulation distortion in fifth-order nonlinear rf circuits/systems. *IEEE Transactions on Microwave Theory and Techniques*, 52(1):121–132, 2004.

[21] Keysight. Cxa signal analyzer. https://www.keysight.com/us/en/product/N9000B/cxa-signal-analyzer-multi-touch-9-khz-26-5-ghz.html, 2018.

[22] Keysight. Ena network analyzer. https://www.keysight.com/us/en/product/E5063A/e5063a-ena-vector-network-analyzer.html, 2020.

[23] Skyworks. Sms7630. https://www.skyworksinc.com/en/Products/Diodes/SMS7630-Series, 2021.

[24] Analog Devices Inc. Max9914. https://www.analog.com/en/products/max9914.html, 2023.

[25] Onsemi. Ncs2200. https://www.onsemi.com/products/signal-conditioning-control/amplifiers-comparators/comparators/ncs2200, 2022.

[26] STMicroelectronics. Stm32u5 series mcu. https://www.st.com/en/microcontrollers-microprocessors/stm32u5-series.html.

[27] Onsemi. 2n3904. https://www.onsemi.com/products/discrete-power-modules/general-purpose-and-low-vcesat-transistors/2n3904, 2019.

[28] Analog Devices Inc. Hmc536. https://www.analog.com/media/en/technical-documentation/data-sheets/hmc536chips.pdf, 2022.

[29] Diodes. Dmg2302. https://www.diodes.com/part/view/DMG2302UK/, 2015.

[30] Zhenqiang Xu. Loraphy. https://github.com/jkadbear/LoRaPHY, 2022.

[31] EBYTE. E32-433t20s lora module. https://www.cdebyte.com/products/E32-433T20S, 2024.

[32] Keysight. Dc power analyzer. https://www.keysight.com/us/en/product/N6705C/dc-power-analyzer-modular-600-w-4-slots.html, 2020.

[33] Analog Devices Inc. Lt5534. https://www.analog.com/en/products/lt5534.html, 2018.

[34] Songfan Li, Hui Zheng, Chong Zhang, Yihang Song, Shen Yang, Minghua Chen, Li Lu, and Mo Li. Passive {DSSS}: Empowering the downlink communication for backscatter systems. In *19th USENIX Symposium on Networked Systems Design and Implementation (NSDI 22)*, pages 913–928, 2022.

[35] Texas Instruments. Tlv9001. https://www.ti.com/product/TLV9001, 2019.

[36] Aaron Parks et al. Wisp5. https://sites.google.com/uw.edu/wisp-wiki/wisp5, 2017.

[37] Daniel M. Dobkin. *The rf in RFID: uhf RFID in practice*. Newnes, 2012.

[38] Fengyuan Ren, Chuang Lin, and Feng Liu. Self-correcting time synchronization using reference broadcast in wireless sensor network. *IEEE Wireless Communications*, 15(4):79–85, 2008.

[39] Pengyu Zhang, Pan Hu, Vijay Pasikanti, and Deepak Ganesan. Ekhonet: High speed ultra low-power backscatter for next generation sensors. In *Proceedings of the 20th annual international conference on Mobile computing and networking*, pages 557–568, 2014.

[40] Songfan Li, Chong Zhang, Yihang Song, Hui Zheng, Lu Liu, Li Lu, and Mo Li. Internet-of-microchips: Direct radio-to-bus communication with spi backscatter. In *Proceedings of the 26th Annual International Conference on Mobile Computing and Networking*, pages 1–14, 2020.

[41] Chong Zhang, Songfan Li, Yihang Song, Qianhe Meng, Minghua Chen, YanXu Bai, Li Lu, and Hongzi Zhu. Lego: Empowering chip-level functionality plug-and-play for next-generation iot devices. In *Proceedings of the 28th ACM International Conference on Architectural Support for Programming Languages and Operating Systems, Volume 3*, pages 404–418, 2023.

[42] Jagdish Pandey, Jianlei Shi, and Brian Otis. A 120μw mics/ism-band fsk receiver with a 44μw low-power mode based on injection-locking and 9x frequency multiplication. In *2011 IEEE International Solid-State Circuits Conference*, pages 460–462. IEEE, 2011.

[43] Nitz Saputra and John R Long. A fully integrated wideband fm transceiver for low data rate autonomous systems. *IEEE journal of solid-state circuits*, 50(5):1165–1175, 2015.

[44] Joshua F Ensworth, Alexander T Hoang, and Matthew S Reynolds. A low power 2.4 ghz superheterodyne receiver architecture with external lo for wirelessly powered backscatter tags and sensors. In *2017 IEEE International Conference on RFID (RFID)*, pages 149–154. IEEE, 2017.

[45] Vivek Mangal and Peter R Kinget. A wake-up receiver with a multi-stage self-mixer and with enhanced sensitivity when using an interferer as local oscillator. *IEEE Journal of Solid-State Circuits*, 54(3):808–820, 2019.

[46] Mohammad Rostami, Karthik Sundaresan, Eugene Chai, Sampath Rangarajan, and Deepak Ganesan. Redefining passive in backscattering with commodity devices. In *Proceedings of the 26th Annual International Conference on Mobile Computing and Networking*, pages 1–13, 2020.

[47] Carlos Pérez-Penichet, Claro Noda, Ambuj Varshney, and Thiemo Voigt. Battery-free 802.15. 4 receiver. In *2018 17th ACM/IEEE International Conference on Information Processing in Sensor Networks (IPSN)*, pages 164–175. IEEE, 2018.

[48] Yihang Song, Li Lu, Jiliang Wang, Chong Zhang, Hui Zheng, Shen Yang, Jinsong Han, and Jian Li. {μMote}: Enabling passive chirp despreading and {μW-level}{Long-Range} downlink for backscatter devices. In *20th USENIX Symposium on Networked Systems Design and Implementation (NSDI 23)*, pages 1751–1766, 2023.

[49] Mehrdad Hessar, Ali Najafi, and Shyamnath Gollakota. {NetScatter}: Enabling {Large-Scale} backscatter networks. In *16th USENIX Symposium on Networked Systems Design and Implementation (NSDI 19)*, pages 271–284, 2019.

[50] Yihang Song, Chao Song, Li Lu, Shen Yang, Songfan Li, Chong Zhang, Qianhe Meng, Xiandong Shao, and Haili Wang. Chipnet: Enabling large-scale backscatter network with processor-free devices. *ACM Transactions on Sensor Networks*, 18(4):1–26, 2022.

[51] Vincent Liu, Aaron Parks, Vamsi Talla, Shyamnath Gollakota, David Wetherall, and Joshua R Smith. Ambient backscatter: Wireless communication out of thin air. *ACM SIGCOMM computer communication review*, 43(4):39–50, 2013.

[52] Maolin Zhang, Si Chen, Jia Zhao, and Wei Gong. Commodity-level ble backscatter. In *Proceedings of the 19th Annual International Conference on Mobile Systems, Applications, and Services*, pages 402–414, 2021.

[53] Muhammad Sarmad Mir, Borja Genoves Guzman, Ambuj Varshney, and Domenico Giustiniano. Passivelifi: Rethinking lifi for low-power and long range rf backscatter. In *Proceedings of the 27th Annual International Conference on Mobile Computing and Networking*, pages 697–709, 2021.

[54] Peter Oppermann and Christian Renner. Higher-order modulation for acoustic backscatter communication in metals. In *Proceedings of the ACM SIGCOMM 2022 Conference*, pages 576–587, 2022.

[55] Haofan Lu, Mohammad Mazaheri, Reza Rezvani, and Omid Abari. A millimeter wave backscatter network for two-way communication and localization. In *Proceedings of the ACM SIGCOMM 2023 Conference*, pages 49–61, 2023.

[56] Bill Tao, Emerson Sie, Jay Shenoy, and Deepak Vasisht. Magnetic backscatter for in-body communication and localization. In *Proceedings of the 29th Annual International Conference on Mobile Computing and Networking*, pages 1–15, 2023.

[57] Aline Eid, Jack Rademacher, Waleed Akbar, Purui Wang, Ahmed Allam, and Fadel Adib. Enabling long-range underwater backscatter via van atta acoustic networks. In *Proceedings of the ACM SIGCOMM 2023 Conference*, pages 1–19, 2023.

[58] Guochao Song, Hang Yang, Wei Wang, and Tao Jiang. Reliable wide-area backscatter via channel polarization. In *IEEE INFOCOM 2020-IEEE Conference on Computer Communications*, pages 1300–1308. IEEE, 2020.

[59] Mastooreh Salajegheh, Shane S Clark, Benjamin Ransford, Kevin Fu, and Ari Juels. Cccp: Secure remote storage for computational rfids. In *USENIX Security Symposium*, pages 215–230, 2009.

[60] Saman Naderiparizi, Mehrdad Hessar, Vamsi Talla, Shyamnath Gollakota, and Joshua R Smith. Towards {Battery-Free}{HD} video streaming. In *15th USENIX Symposium on Networked Systems Design and Implementation (NSDI 18)*, pages 233–247, 2018.

[61] Chong Zhang, Songfan Li, Yihang Song, Qianhe Meng, Hongzi Zhu, Xin Wang, et al. A lightweight and chip-level reconfigurable architecture for next-generation iot end devices. *IEEE Transactions on Computers*, 2023.

[62] Songfan Li, Qianhe Meng, Yanxu Bai, Chong Zhang, Yihang Song, Shengyu Li, and Li Lu. Go beyond rfid: Rethinking the design of rfid sensor tags for versatile applications. In *Proceedings of the 29th Annual International Conference on Mobile Computing and Networking*, pages 1–16, 2023.

[63] Hongyu Lu, Ahmed G Gadelkarim, Jiannan Huang, and Patrick P Mercier. A 0.69-mw sub-sampling nb-iot receiver employing a linearized q-boosted lna. *IEEE Open Journal of the Solid-State Circuits Society*, 2024.

[64] Hossein Pirayesh, Shichen Zhang, Pedram Kheirkhah Sangdeh, and Huacheng Zeng. Maloragw: Multi-user mimo transmission for lora. In *Proceedings of the 20th ACM Conference on Embedded Networked Sensor Systems*, pages 179–192, 2022.

[65] Xianjin Xia, Ningning Hou, Yuanqing Zheng, and Tao Gu. Pcube: scaling lora concurrent transmissions with reception diversities. *ACM Transactions on Sensor Networks*, 18(4):1–25, 2023.

[66] Ningning Hou, Xianjin Xia, and Yuanqing Zheng. Don't miss weak packets: Boosting lora reception with antenna diversities. *ACM Transactions on Sensor Networks*, 19(2):1–25, 2023.

[67] Amalinda Gamage, Jansen Liando, Chaojie Gu, Rui Tan, Mo Li, and Olivier Seller. Lmac: Efficient carrier-sense multiple access for lora. *ACM Transactions on Sensor Networks*, 19(2):1–27, 2023.